

## OPTIMAL DETERMINATION OF DETECTOR PLACEMENT IN CEREBRAL NIR SPECTROSCOPY OF NEONATES USING CHEMOMETRIC TECHNIQUES

Terence S. Leung, Clare E. Elwell, and David T. Delpy

**Abstract:** This paper investigates the optimal placement of NIRS optodes in order to maximise the detection of haemoglobin changes in cortical grey matter resulting from an evoked response in neonates. The analysis is based upon predictions of optical signal at the surface of the head, using a Finite Element based model of light diffusion in tissue. Using the generated intensity data, the combination of optode positions, which maximise the signal from cortical grey matter whilst minimising that from surface tissue or cerebral white matter, is determined using a Chemometric statistical analysis. The neonatal head is modelled as a 2-dimensional circle with 3 layers corresponding to the skin/scalp, and grey and white matter. A wide range of absorption coefficients for each layer is simulated, based upon physiologically reasonable values for parameters. Surface intensity at 10 different optode positions have been generated for a total of 31,250 combinations of these variables for the 3 layers. It was found that with 3 optodes at 5, 15, and 50 mm apart from the source, the smallest root-mean-square error between the estimated and modelled values can be obtained. Increasing the number of optodes further does not improve the performance.

### 1. INTRODUCTION

Non-invasive near infrared (NIR) spectroscopy measurement is widely used in investigating the cerebral oxygenation and haemodynamics in humans. However, it is known that the measurements obtained from the surface of a human head are not totally comprised of intracerebral signals, but also contain extracerebral signals from the skin and skull. It has also been shown that the mean interrogation depth of photons increases with increasing optode spacing,<sup>1</sup> resulting in different signal contributions from skin,

skull, and cerebral grey and white matter as a function of optode spacing. As illustrated schematically in Figure 1, detector 1 predominantly measures the attenuation ( $A_1$ ) through skin/skull, detector 2 measures  $A_2$ , which includes some signals from the grey matter, and detector 3 measures  $A_3$ , which further includes some white matter contribution. Signals purely from the brain are clinically useful, and several schemes have been proposed to minimise the contamination from extracerebral tissues by subtraction of signals measured at different optode spacings.<sup>2</sup> Generalising this methodology, we investigated the optimal number and positions of detectors on a neonatal head to maximise the detection of total haemoglobin concentration change in the cortical grey matter where evoked responses occur. To achieve this aim through experiment would require measurements of optical signals (e.g. intensity or mean time) at all points on the surface whilst systematically changing the optical properties (i.e. absorption ( $\mu_a$ ) and scattering ( $\mu_s'$ ) coefficient) of each tissue layer. With prior knowledge of the actual grey matter haemoglobin concentration which determines  $\mu_a$ , the optimal number and positions of detectors can then be determined by a chemometric technique known as Partial Least Square (PLS). In practice, such experimental measurements are not possible in human or animal subjects, and using experimental phantoms would be difficult and require a very large number of studies. This paper therefore presents a computer simulation to tackle this issue.

## 2. THEORY

### 2.1. Maximising Intracerebral Signals by the Weighted Sum of Surface Measurements

The attenuation caused by absorption at a particular layer can be approximated by the partial differential pathlength<sup>3</sup> (PDP), which is the mean pathlength photons travel in that layer. The attenuation measured by detectors 1-3 in the example shown in Figure 1A can be written as:

$$\Delta A_n(\lambda) = L_n^{skin} \Delta \mu_a^{skin}(\lambda) + L_n^{grey} \Delta \mu_a^{grey}(\lambda) + L_n^{white} \Delta \mu_a^{white}(\lambda) \quad (1)$$

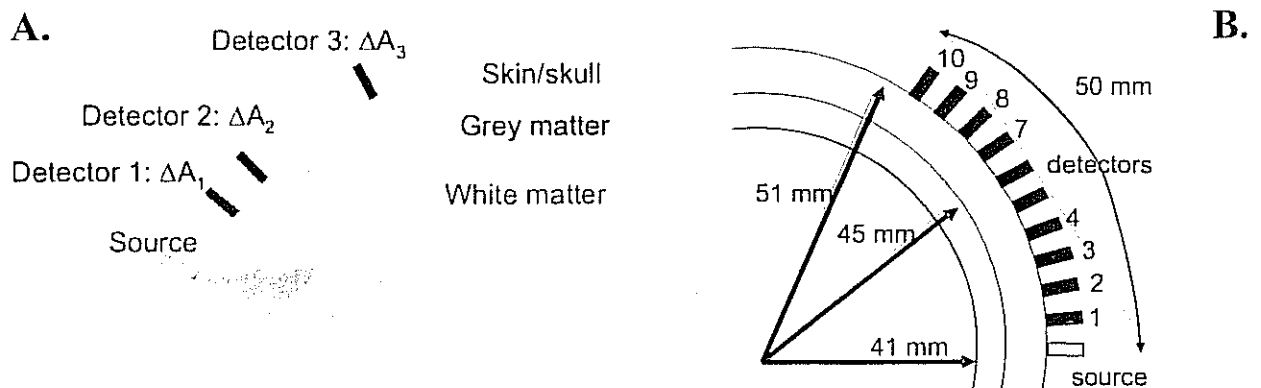


Figure 1. A. Light paths in different source detector spacings. B. Model dimension and positions of source and detectors.

where  $\Delta\mu_a(\lambda)$  is the change in  $\mu_a$ ,  $\Delta A_n(\lambda)$  and  $L_n$  are the change in attenuation, and the PDP is measured by the detector  $n$ . In the example of Figure 1,  $L_1^{grey} = L_1^{white} = L_2^{white} = 0$ . Generally speaking, there exists a weighted sum of  $\Delta A_n(\lambda)$  that maximises  $\Delta\mu_a(\lambda)$  from a particular layer (the grey matter, in this case),

$$\Delta\mu_a^{grey}(\lambda) = \sum_{n=1}^N w_n^\lambda \Delta A_n(\lambda) \quad (2)$$

where  $w_n^\lambda$  is the weighting given to  $\Delta A_n(\lambda)$  measured by detector  $n$  at wavelength  $\lambda$  ( $w_n^\lambda$  can also be expressed as a function of PDP in certain layers), and  $N$  is the number of detectors. In this work, the total haemoglobin concentration in the grey matter is the target, which can be written as (in this case, using two wavelengths):

$$\Delta[HbT]^{grey} = \Delta[HbO_2]^{grey} + \Delta[HHb]^{grey} = (k_{11} + k_{12})\Delta\mu_a^{grey}(\lambda_1) + (k_{21} + k_{22})\Delta\mu_a^{grey}(\lambda_2) \quad (3)$$

where  $\Delta[HbT]^{grey}$ ,  $\Delta[HbO_2]^{grey}$ ,  $\Delta[HHb]^{grey}$  correspond to changes in the total, oxy- and deoxy-haemoglobin concentrations in the grey matter, and  $k_{ij}$  is the element of the inverse of the matrix containing the specific absorption coefficients of  $HHb$  and  $HbO_2$ , respectively. Substituting (2) into (3), the following can be written:

$$\Delta[HbT]^{grey} = \sum_{n=1}^N \left[ b_n^{\lambda_1} \Delta A_n(\lambda_1) + b_n^{\lambda_2} \Delta A_n(\lambda_2) \right] \quad (4)$$

where  $b_n^{\lambda_1} = (k_{11} + k_{12})w_n^{\lambda_1}$  and  $b_n^{\lambda_2} = (k_{21} + k_{22})w_n^{\lambda_2}$ .

## 2.2. Modelling Light Transport

Light transport has been modelled by the diffusion theory implemented in a finite element method (FEM),<sup>4</sup> which has been verified against Monte Carlo and phantom experiments. This light transport modelling is part of a software package known as Time-resolved Optical Absorption and Scattering Tomography (TOAST) developed to perform light transport modelling and tomographic image reconstruction. TOAST provides fast computation, which is crucial in this study because of the need to generate thousands of datasets. The neonatal head is modelled as a 2 dimensional circle with 3 layers corresponding to the skin/scalp (radius = 51 mm), grey matter (radius = 45 mm), and white matter (radius = 41 mm). The FEM mesh consists of 25,327 nodes and 12,474 elements. Because of signal:noise considerations, practical NIRS measurements are typically limited to optode spacings of about 50mm, and this limitation has been included in the model. The resulting locations of the source and 10 detectors are shown in Figure 1B. The first detector is 5 mm from the source, and subsequent detectors are 5 mm apart.

## 2.3. Physiological Changes in Each Layer

A wide range of  $\mu_a$  for each layer is simulated, based upon physiologically reasonable values for parameters such as the total haemoglobin concentration ( $HbT$ ), in

Table 1. Summary of modelled parameter variations.

Layer	Parameters	Range (min:step:max)
Skin/scalp (layer 1)	HbT conc ( $\mu\text{M}$ )	30:10:70
	Tissue Oxygenation (%)	50:10:90
Grey Matter (layer 2)	HbT conc ( $\mu\text{M}$ )	60:10:100
	Tissue Oxygenation (%)	50:10:90
White Matter (layer 3)	HbT conc ( $\mu\text{M}$ )	20:10:60
	Tissue Oxygenation (%)	50:10:90

$\mu\text{M}$ ), tissue blood oxygenation ( $TO$ , in fractional %), water content ( $W$ , in fractional %), and background absorption ( $B$ , in  $\text{mm}^{-1}$ ). The variations in parameters are summarised in Table 1. The  $\mu_a$  of each layer is calculated as follows:

$$\mu_a(\lambda) = \varepsilon_{HHb}(\lambda)HbT(1 - TO) + \varepsilon_{HbO_2}(\lambda)HbT \cdot TO + \mu_{a,H_2O}(\lambda)W + B \quad (5)$$

where  $\varepsilon_{HHb}(\lambda)$ ,  $\varepsilon_{HbO_2}(\lambda)$  are the specific absorption coefficients of  $HHb$  and  $HbO_2$ ,  $\mu_{a,H_2O}(\lambda)$  is the  $\mu_a$  of 100% water, and  $B$  is a wavelength independent background absorption. The transport scattering coefficient ( $\mu_s'$ ) and background absorption are fixed at  $1 \text{ mm}^{-1}$  ( $\lambda = 780 \text{ nm}$ ) and  $0.003 \text{ mm}^{-1}$  (at all wavelengths), respectively, for all three layers, while the tissue water contents are set at 70% in skin/scalp and 80% in the grey and white matter. A summary of variations of modelled parameters is given in Table 1. The wavelength dependency of  $\mu_s'$  is also included<sup>5</sup>; for example, when  $\mu_s'$  (780 nm) is  $1 \text{ mm}^{-1}$ ,  $\mu_s'$  (820nm) is scaled to  $0.9534 \text{ mm}^{-1}$ .

#### 2.4. Optimization by Chemometric Techniques

Given a target and a set of measurements that are influenced by other factors, chemometric techniques such as PLS seek to optimise the estimation of the target by weighting the measurements optimally. Equation (4) can be re-written in matrix form as:

$$\mathbf{y} = \mathbf{X}\mathbf{b} \quad (6)$$

where  $\mathbf{y}$  is the target,  $\mathbf{X}$  a set of measurements, and  $\mathbf{b}$  the optimal weightings. In our case,  $\mathbf{y}$  is the total haemoglobin concentration in the grey matter (i.e.  $\Delta[HbT]^{grey}$ ), and  $\mathbf{X}$  is a set of measurements (e.g.  $\Delta A_n(\lambda)$ ) from 10 (or fewer) detectors at two wavelengths, i.e.

$$\mathbf{X} = \begin{bmatrix} \Delta A_1(\lambda_1, t_1) & \cdots & \Delta A_N(\lambda_1, t_1) & \Delta A_1(\lambda_2, t_1) & \cdots & \Delta A_N(\lambda_2, t_1) \\ \vdots & & \vdots & \vdots & & \vdots \\ \Delta A_1(\lambda_1, t_M) & \cdots & \Delta A_N(\lambda_1, t_M) & \Delta A_1(\lambda_2, t_M) & \cdots & \Delta A_N(\lambda_2, t_M) \end{bmatrix}$$

$$\mathbf{y} = \begin{bmatrix} \Delta[HbT]^{grey}(t_1) \\ \vdots \\ \Delta[HbT]^{grey}(t_M) \end{bmatrix} \quad \mathbf{b}^T = [\mathbf{b}^{\lambda_1} \quad \mathbf{b}^{\lambda_2}] = [b_1^{\lambda_1} \quad \cdots \quad b_N^{\lambda_1} \quad b_1^{\lambda_2} \quad \cdots \quad b_N^{\lambda_2}] \quad (7)$$

In PLS, the optimal weighting,  $\mathbf{b}$ , can be considered as a projection of the original measurements on to a new plane with a given number of principle components. This approach captures the largest amount of variance in  $\mathbf{X}$  and at the same time optimises the correlation between  $\mathbf{X}$  and  $\mathbf{y}$ . More details can be found in the literature.<sup>6</sup>

### 3. METHODS

#### 3.1. Data Generation

As shown in Table 1, the values of six variables were changed one by one with 5 steps between the minimum and maximum values in the range, resulting in 15,625 ( $\equiv 5^6$ ) sets of data. Each data set was generated by TOAST and contained estimates of intensity and mean time at the 10 detector positions shown in Figure 1B. All NIRS instruments are equipped with at least 2 laser sources with wavelengths at both sides of the isobestic point (800 nm). We therefore also generated the intensity and mean time data at two wavelengths (780 & 820 nm) to simulate the practical situation. In this initial study, only intensity data were included in the analysis, and the intensity measurements ( $I$ ) were converted to attenuations by the conventional formulation:  $A = -\log_e(I)$ .

#### 3.2. Calibration with Partial Least Square

The data  $[HbT]^{grey}$  and  $A_n(\lambda)$  were scaled to zero mean and unit variance. These data can thus be considered as changes from their mean values, i.e.  $\Delta[HbT]^{grey}$  and  $\Delta A_n(\lambda)$ . The aim of this work is to find the best combination of detectors given, say,  $P$  detectors, e.g. if 3 detectors are to be chosen out of the 10 detectors in Figure 1B, the possible combinations will include detectors 1, 2, 3; detectors 1, 2, 4; detectors 1, 2, 5 and so on. The total possible number of combinations can be found by the binomial coefficient,  ${}^P C_N = P!/[N!(P-N)!]$ , in which  $N$  elements are selected from  $P$  elements. For this example, the total number of combinations is  ${}_{10}C_3 = 120$ . For each combination of detectors, the corresponding measurements,  $\Delta A_n(\lambda)$  and  $\Delta[HbT]^{grey}$ , were used as  $\mathbf{X}$  and  $\mathbf{y}$ , respectively, in the basic model in Eq. (6). Using PLS with 3 principle components, the weighting of  $\mathbf{b}$  was found. Subsequently, the root-mean-square (RMS) value between the actual and predicted  $\Delta[HbT]^{grey}$  was calculated and used as a performance measure. Analyses were carried out based on  $P = 10$  and  $N = 1, 2, 3, 4, 6,$  and  $10$ . It should be noted that for 1 detector, the analysis was performed using multiple linear regression instead of PLS.

### 4. RESULTS

Table 2 summarises the results in terms of minimum RMS errors obtained by the optimal combination of  $N$  detectors out of a total of 10 ( $P$ ) detectors. With only one detector, which is a common setup for many commercial NIRS instruments, the RMS error is the largest at 12.9  $\mu\text{M}$  (real concentration varying from 60 to 100  $\mu\text{M}$ ). With two and three detectors, the RMS errors have been reduced to 4.0 and 1.6  $\mu\text{M}$ , respectively.

**Table 2.** Minimum RMS errors obtained by the optimal combination of  $N$  detectors.

Number of detectors ( $N$ )	Optimal position of detectors (refer to Figure 2)	Minimum RMS error ( $\mu\text{M}$ )
1	8	12.9
2	1, 2	4.0
3	1, 3, 10	1.6
4	1, 2, 3, 10	1.6
6	1, 2, 4, 9, 10	1.6
10	1, 2, 3, 4, 5, 6, 7, 8, 9, 10	1.8

With more detectors for  $N = 4, 6, 10$ , the RMS errors are not reduced further. The weightings  $b^{\lambda_1}$  [ $\lambda_1=780$  nm, refers to Eq. (7)] for  $N = 2, 3, 4, 6, 10$  are shown in Figure 2. The weightings  $b^{\lambda_2}$  ( $\lambda_2=820$  nm) have similar relative values and are not shown.

## 5. DISCUSSION AND CONCLUSIONS

For neonatal measurements, when only a single detector is available, the optimal position of this detector is 40 mm from the source (detector 8), in agreement with the literature.<sup>7</sup> Figure 2 shows the relative signal weightings that resulted from PLS analysis for 2, 3, 4, 6, and 10 detectors and provides some intuitive insight into the logic behind the calibration. The closest detectors pick up more photons that have travelled through the skin/skull, whose contribution is to be minimised, and hence have a negative weighting. A relatively higher proportion of photons measured over the next few detectors also pass through the grey matter and hence have a rather larger positive weighting. Detectors further away receive photons that have travelled through the white matter (in addition to the first two layers), whose contribution is also minimised by negative weightings. In an  $N$  layer model, the absorption change in a particular layer can be calculated if  $N$  number of surface measurements are available. As briefly discussed in section 2.1., this is because one can always express the absorption change in a particular

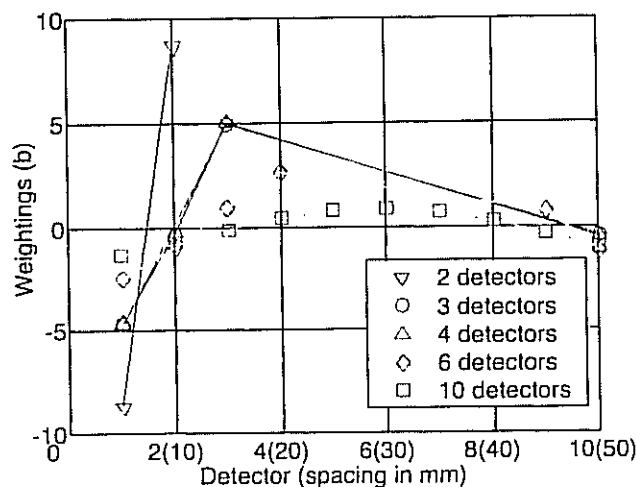


**Figure 2.** The optimal weighting  $b^{\lambda_1}$  for different number of detectors at 780 nm.

layer with the weighted sum of  $N$  surface measurements. This is, however, only true if we limit our discussion of the effects of inhomogeneity in terms of PDP,<sup>3</sup> which is a linear approximation. In a more realistic non-linear diffusion theory based model such as the one simulated by the TOAST software, one should not expect the weighted sum to be totally due to absorption change in one particular layer alone. When at least two wavelengths are available, the total haemoglobin concentration change can be obtained as described in Eq. (4). The minimum RMS error is obtained with 3 or more detectors, which agrees with the above discussion that at least 3 (or  $N$ ) detectors are needed for a 3 (or  $N$ ) layer model, although it is interesting that virtually no improvement in RMS error results from inclusion of further detectors. Analyses based on the mean time measurements also show similar results: that 3 detectors are sufficient to minimise the RMS error and that additional detectors do not further improve the performance. Due to the constraint of space, more details cannot be discussed here. The simplified model of the head used here does not include a cerebrospinal fluid (CSF) layer, which is known to affect light distribution. This is justified in the case of the neonatal head where the CSF layer is thin (0.5 – 1.0 mm) and the scattering coefficient of the white matter in the neonatal brain is lower than that in an adult brain because of reduced myelination. However, it is anticipated that the presence of CSF and local thickness variation, as would be required in a more realistic adult brain model, would change the way light propagates, and in this instance a hybrid diffusion/radiosity model<sup>8</sup> would need to be employed. In this case, the optimal number of detectors that results in the minimum prediction error would also depend on the underlying number of layers, and the optimal locations of the detectors may also be significantly different. However, the general analysis methodology described here should still apply.

## 6. ACKNOWLEDGEMENTS

The authors thank Dr. A. Gibson, Dr. J. Riley, and Prof. S. Arridge for their help in running the simulations and useful comments. This work was funded by the Wellcome Trust, EPSRC, and Hamamatsu Photonics KK.

## REFERENCES

1. G. H. Weiss, R. Nossal, and R. F. Bonner, Statistics of penetration depth of photons re-emitted from irradiated tissue, *J. Mod. Opt.* **36**, 349-359 (1989).
2. P. W. McCormick, M. Stewart, M. G. Goetting, M. Dujovny, G. Lewis, and J. I. Ausman, Noninvasive cerebral optical spectroscopy for monitoring cerebral oxygen delivery and hemodynamics, *Crit. Care Med.* **19**, 89-97 (1991).
3. M. Hiraoka, M. Firbank, M. Essenpreis, M. Cope, S. R. Arridge, P. van der Zee, and D. T. Delpy, A Monte Carlo investigation of optical pathlength in inhomogeneous tissue and its application to near-infrared spectroscopy, *Phys. Med. Biol.* **38**, 1859-1876 (1993).
4. S. R. Arridge, M. Schweiger, M. Hiraoka, and D. T. Delpy, A finite element approach for modelling photon transport in tissue, *Med. Phys.* **20**, 299-309 (1993).
5. S. J. Matcher, M. Cope, and D. T. Delpy, In vivo measurements of the wavelength dependence of tissue-scattering coefficients between 760 and 900 nm measured with time-resolved spectroscopy, *App. Opt.* **36**, 386-396 (1997).
6. H. Martens, and T. Naes, *Multivariate Calibration*, (John Wiley & Sons Ltd, UK, 1991).
7. S. Kohri, Y. Hoshi, M. Tamura, C. Kato, Y. Kuge, and N. Tamaki, Quantitative evaluation of the relative contribution ratio of cerebral tissue to near-infrared signals in the adult human head: a preliminary study, *Physiol. Meas.* **23**, 301-312 (2002).
8. M. Firbank, S. R. Arridge, M. Schweiger, and D. T. Delpy, An investigation of light transport through scattering bodies with non-scattering regions, *Phys. Med. Biol.* **41**, 767-783 (1996).